High-fidelity simulations of thin shell deployable structures with adaptive meshing

F Gianfranco Canales* and Sergio Pellegrino†

California Institute of Technology, Pasadena, CA, 91125

An adaptive meshing procedure is developed for the analysis of thin shell structures that experience localized elastic deformations associated with the formation of folds. The refinement criterion for remeshing takes into consideration the localization of deformation in the folds, while avoiding excessive refinement outside this region. The local bending strains in two principal directions are used to construct the refinement criterion. A geometrical parameter related to a boundary layer effect is shown to be effective as a limit length for refinement. Isogeometric shell finite elements are used for the simulations. Different tape spring geometries are simulated to illustrate the generality and efficiency of the proposed adaptive procedure.

Nomenclature

E	=	Young's modulus
h_i	=	Element length along axis i
h_{th}	=	Element length limit
L	=	Tape spring length
M^{max}	=	Peak moment
M^*	=	Steady-state moment
R	=	Radius of curvature
r_i	=	Refinement indicator
r_0	=	Refinement threshold
t	=	Thickness
α	=	Arc angle
κ_i	=	Bending strain along axis i
ν	=	Poisson's ratio

I. Introduction

Ultralight deployable structures have been proposed for various space applications, such as solar power [1] and RF antennas [2]. Complex space structures that use long and narrow thin-shell structural elements are envisaged. The longerons can be coiled and deployed as necessary, and during packaging they experience localized deformations (folds) [3]. These folds can form suddenly and are fundamental to understanding and simulating the deployment process.

The finite element method [4] has been developed as a means of simulating complex structures. It applies the differential equations of equilibrium in weak form by discretizing the structure into a mesh of finite elements. Although the method can describe the behavior of structures accurately, it can be computationally intensive as the size of the discretisation depends on the size of the structure and the characteristics of the deformation. The use of non-uniform meshes can improve the efficiency of the method [5]. The mesh can be modified as the solution progresses, in order to obtain accurate results with minimal computational cost, which is denoted as adaptive meshing. The refinement can be guided by defining an error estimator [6]. Although bounds on the errors and robust estimators are available for linear problems, in nonlinear problems the accuracy of error estimators can be problem-dependent and lacks robustness. Another approach for adaptive meshing is to define refinement indicators for each element. Elements are selected for refinement according to whether the refinement indicator exceeds a certain threshold value. The values of the refinement

---

*Graduate Student, Graduate Aerospace Laboratories, 1200 E California Blvd, Pasadena. E-mail: fcanales@caltech.edu

†Joyce and Kent Kresa Professor of Aeronautics and Civil Engineering, Graduate Aerospace Laboratories, 1200 E California Blvd. MC 105-50, Pasadena. AIAA Fellow.

indicators are used to mark specific elements for refinement. Different refinement indicators have been proposed in the literature, based on the strain energy [7], the gradient of the strain energy [8], and a measure of the curvature vector [9].

Adaptive procedures have been mostly developed for standard finite elements. These elements use shape functions which exactly interpolate values at nodes. Although mathematically simple, more complex shape functions could allow various advantages to be realised. Isogeometric finite elements [10] use the same shape functions as the geometries defined in computer-aided design software, that is, Non-Uniform Rational B-Spline (NURBS) shape functions. These functions can model certain geometric features exactly, such as cylinders. However, NURBS functions have a tensor product structure, and thus a rectangular mesh grid must be used. This makes truly local refinement impossible. Extensions of the isogeometric analysis to other shape functions that increase the mesh flexibility are available, such as T-splines [11]. Adaptive meshing using T-splines has been developed [12], [13] and is useful when highly local effects are present. However, the meshing procedure is significantly more complex than with NURBS functions.

In this work, we present a new adaptive meshing procedure for deployable thin shell structures. Two refinement indicators per element are used, each of which marks the element for refinement along an axis in the local shell coordinate system. As a test case, we consider a tape spring, which is a long and thin cylindrical shell that exhibits similar localized deformations observed in complex thin-shell deployable structures. Simulations are performed using the isogeometric shell finite element formulation presented in [14]. In order to limit excessive refinement in the fold region, a limit to the refinement is introduced by defining an element length lower limit. This limit is derived from an estimate of the boundary layer in tape springs [3]. This approach is shown to be efficient for tape springs with various geometries.

II. Tape spring geometry and behavior

A tape spring can be described as a cylindrical shell of length L, thickness t, radius of curvature R and angle subtended α, as shown in Fig. 1.
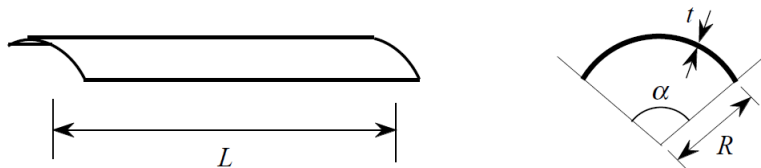

Fig. 1   Tape spring geometry [15].

The tape spring is subjected to opposite-sense bending moments that deform the shell as shown in Fig. 2. As the moment is increased, the initially smooth deformation becomes localized, and a fold forms at the center. Both stages of this process are illustrated in Fig. 2.
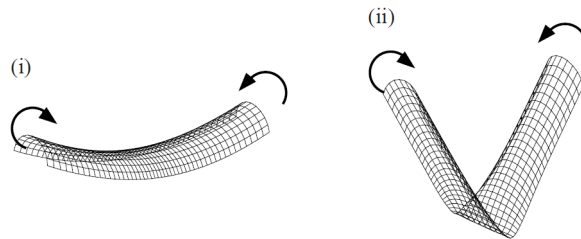

Fig. 2   Opposite-sense bending [15]. (i) Smooth beam-like bending. (ii) Localized fold formation.

This process can be characterized by plotting the relation between the moment reaction at the ends and the rotation applied. A schematic diagram of this relationship is shown in Fig. 3. For small end rotations the moment-rotation relationship is linear. As the rotation is increased, a peak moment, M^{max}, is reached as the cross-section near the center of the tape suddenly flattens. With further rotation increases, the deformation localizes in a small region, and a snap-through behavior occurs between points A and B. If the rotation is increased further, the moment stays almost constant.
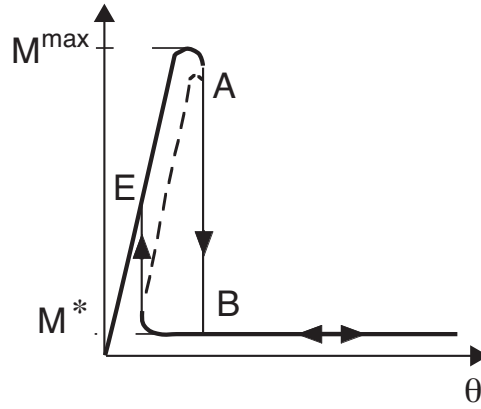
Fig. 3   Moment-rotation schematic relationship.

III. NURBS basis functions for surfaces

Since the isogeometric shape functions dictate the meshing procedure, a brief overview of the bidimensional NURBS basis functions used in the finite element procedure and the B-spline functions which are used as building blocks are presented here. More details are given in [10].

Univariate B-spline basis functions of degree p are constructed by defining a non-decreasing sequence of elements $\{\xi_1, ..., \xi_{n+p+1}\}$, each of which is called a knot. There are n basis function associated with this knot sequence, which can be computed using the Cox-de-Boor recursion formula:

$$N_{i,p}(\xi) = \frac{\xi - \xi_i}{\xi_{i+p} - \xi_i} N_{i,p-1}(\xi) + \frac{\xi_{i+p+1} - \xi}{\xi_{i+p+1} - \xi_{i+1}} N_{i+1,p-1}(\xi) \tag{1}$$

For the case $p = 0$ a piecewise constant basis function is defined:

$$N_{i,0}(\xi) = \begin{cases} 1, & \text{if} \quad \xi_i \le \xi < \xi_{i+1} \\ 0, & \text{otherwise} \end{cases} \tag{2}$$

Bidimensional B-spline basis functions are obtained as a tensor product of sets of univariate B-spline functions. On each dimension we use the variables (ξ^1, ξ^2) respectively, the degrees of the functions (p^1, p^2) and (n^1, n^2) basis functions.

The bidimensional B-spline basis functions are defined as:

$$B_{i,\mathbf{p}}(\boldsymbol{\xi}) = N_{i^1,p^1}\left(\xi^1\right) N_{i^2,p^2}\left(\xi^2\right) \tag{3}$$

where $i = i^1 + n^1(i^2 - 1)$, $\mathbf{p} = \{p^1, p^2\}$, $\boldsymbol{\xi} = (\xi^1, \xi^2)$ and $i^k = \{1, ..., n^k\}$.

Bidimensional NURBS basis functions are defined as:

$$R_{i,\mathbf{p}}(\boldsymbol{\xi}) = \frac{w_i B_{i,\mathbf{p}}(\boldsymbol{\xi})}{\sum_{i=1}^{n} w_i B_{i,\mathbf{p}}(\boldsymbol{\xi})} \tag{4}$$

where $n = n^1 n^2$ and w_i are specified weights.

NURBS sufaces are defined using the NURBS shape functions as follows:

$$\mathbf{S}(\boldsymbol{\xi}) = \sum_{i=1}^{n} \boldsymbol{P}_i R_{i,\mathbf{p}}(\boldsymbol{\xi}) \tag{5}$$

where $\boldsymbol{P}_i \in \mathbb{R}^3$ are control points which form the surface mesh. By carefully choosing the control points $\boldsymbol{P}_i$ and the weights w_i, various surfaces can be obtained.

3

IV. Adaptive meshing procedure

The adaptive procedure is different than for standard finite elements due to the tensor product structure of NURBS shape functions. Refinement in the literature is commonly performed in every axis of a given element, which is not possible when using NURBS shape functions. Therefore, we propose a new adaptive meshing procedure which is suitable for meshes formed by tensor product. This procedure is described by specifying (i) the refinement indicator and (ii) the method for remeshing. Both are defined below.

A. Refinement indicator

This parameter is used to decide whether an element needs to be refined. We propose using one refinement indicator for each direction in the local shell coordinate system. Each refinement indicator r_i is defined using the bending strain κ_i and the element length h_i along the corresponding axis i:

$$r_i = \kappa_i h_i \tag{6}$$

Subdivisions are added along a given element axis if the refinement indicator corresponding to that axis exceeds a threshold value r_0. In addition, we define an element length limit h_{th} at which no further refinement is carried out:

$$\text{IF} \quad \left\{ \begin{array}{c} r_i > r_0 \\ h_i/2 > h_{th} \end{array} \right. \quad \text{REFINE along } i \text{ axis} \tag{7}$$

The element length limit h_{th} is defined as follows:

$$h_{th} = \sqrt{Rt} \tag{8}$$

This parameter is related to the edge effect in tape springs [3]. When there is a fold in a tape spring, there is a transition along the arc axis between the free edges and the central, uniform curvature region. The parameter h_{th} describes this transition length.

B. Remeshing scheme

When the refinement indicator r_i exceeds the threshold value r_0, the element is marked for refinement. We refine the element along the axis i by introducing subdivisions. For example, consider the mesh in Figure 4a. If the top two elements are considered for refinement along the horizontal axis, we introduce the subdivision shown in Figure 4b. If the same two elements are considered for refinement along the vertical axis, we introduce subdivisions such as those shown in Figure 4c.
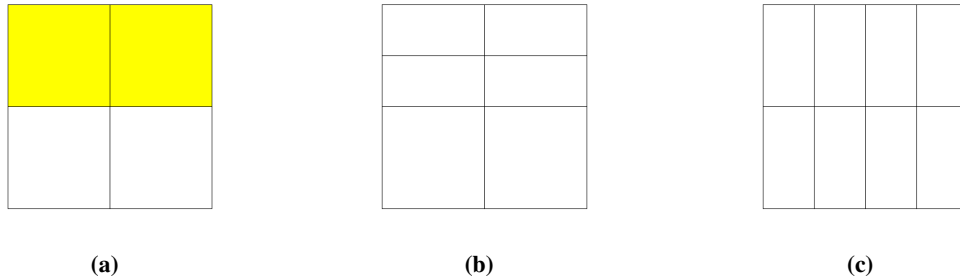

(a)   (b)   (c)

Fig. 4 Refined meshes. (a) Initial mesh with elements marked for refinement in yellow. (b) Subdivisions along horizontal direction. (c) Subdivisions along vertical direction.

.

Note that this type of remeshing (where the additional subdivision lines extend through the whole mesh) is necessary due to the grid structure of the NURBS shape functions used in the simulation. However, due the particular nature of the folds in tape springs (which drive the adaptive meshing), this proposed adaptive meshing procedure is still efficient. Further work will examine the use of T-spline shape functions [11], which can account for hanging nodes and therefore do not need extension of subdivision lines through the whole mesh.

4

After the finer mesh is defined, the displacement data in the coarse mesh is interpolated to the fine mesh using the NURBS shape functions. However, the interpolated displacement data does not in general satisfy the equilibrium equations defined with the fine mesh. Therefore, a new equilibrium is solved for using the Newton-Raphson method. This is done with the load level fixed at the value from the previous step. Due to the presence of snap-through behavior in tape springs, the standard Newton-Raphson solver might fail. Therefore, a backtracking line search [16] is added to the Newton-Raphson scheme to increase robustness.

V. Numerical results

Tape springs of various geometries are tested using the adaptive procedure described above. The refinement indicator threshold r_0 is found by a calibration procedure, evaluating the error of a coarse mesh by comparing with results from a fine mesh for a few load steps. We stop this procedure when the error of the coarse mesh exceeds 1%, and the maximum value of the refinement indicator r_i given in Eq. (6) is taken as the threshold. We observed that this value only changes very slightly when different tape spring geometries are used, so it is assumed constant. Using this method, the refinement indicator threshold is chosen to be $r_0 = 0.019$.

The Newton-Raphson solver is used, using the rotation applied at the ends as the incremental variable. The total rotation applied is chosen to be high enough to observe the snap-through behavior. The rotation increment at each step is fixed, and dependent on the tape spring geometry. The same step is used for both results using a uniform mesh and the adaptive mesh procedure. A geometrically nonlinear isogeometric shell element formulation [14] has been implemented in MATLAB using GPU commands and is used to carry out the analysis. Computations are performed using a laptop with Intel i7-8750H processor, 16 GB RAM and a GeForce GTX 1070 GPU. Results from ABAQUS/Standard 2018 finite element software using shell elements S4 and the arc-length method [17] are used for reference.

An isotropic tape spring is considered in the following. It has Young's modulus $E = 131$ GPa and Poisson's ratio $\nu = 0.3$. The angle subtended by the cross-section is $\alpha = 110°$.

A. Baseline case

Initially, we consider a tape spring with the geometrical parameters $L = 300$ mm, $R = 10$ mm and $t = 0.1$ mm. The initial mesh of the tape spring contains 4 elements along the length and 4 elements along the arc. Using Eq. (8), the element length limit for the adaptive procedure is $h_{th} = 1$ mm.

The initial and final states of deformation of the tape spring are shown in Figure 5, where the formation of a localized deformation at the center is evident. Using the adaptive procedure we obtain the results shown in Figure 6. Results from ABAQUS are also shown to ascertain the accuracy of the uniform fine mesh. Good accuracy is observed compared to results from ABAQUS and results from a fine mesh. Meshes used at different rotation angles are shown in Figure 7, as well as the uniform fine mesh used for comparison.

It should be noted that after the snap-through behavior occurs (at around 10° of rotation of the ends) the mesh does not have further changes and remains constant until the end, indicating that bending strains do not increase further. Also, the number of elements along the arc is the same at the end of the adaptive procedure as with the uniform mesh. However, the number and distribution of elements along the length of the tape spring differs.

B. Influence of length

We tested the adaptive procedure for tape springs of two different lengths: $L = 150$ mm, and $L = 600$ mm keeping the radius and thickness the same as before. We plot the results using the adaptive meshing method and the results obtained using a uniform fine mesh as a reference in Fig. 8. Good agreement is observed in both cases. The steady-state moment is almost the same in both cases, which agrees with the analytical results from [15].

The speedup factor of the adaptive procedure compared to using a uniform mesh with similar accuracy is given in Table 1. This includes time spent remeshing and finding a new equilibrium solution after remeshing. With longer lengths, the fold that is created in the tape spring becomes a smaller part of the total structure and is more localized. This is shown in Figure 9, where the final deformation state for the two tape spring geometries are presented. Due to the more localized nature of the fold as the tape spring is longer, the adaptive procedure is more efficient.

C. Influence of radius and thickness

We know consider tape springs with $L = 300$ mm and two sets of radii and thicknesses given in Table 2. Using Eq. (8), the element length limit is $h_{th} = 0.95$ mm for both geometries. The initial mesh is the same as before, with 4
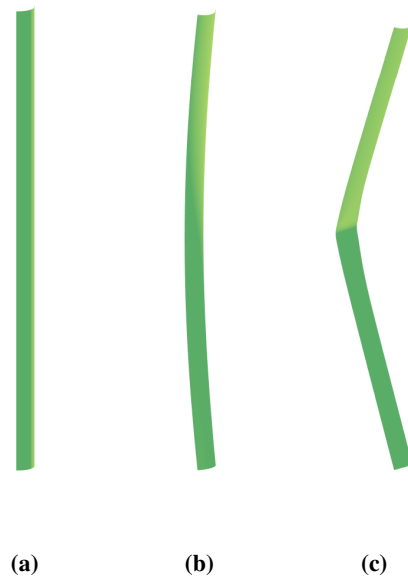
5

(a)   **(b)**   **(c)**

Fig. 5   **Tape spring with parameters $L = 300$ mm, $R = 10$ mm and $t = 0.1$ mm. (a) Initial state. (b) Deformed state before snap-through. (b) Final deformed state.**

elements along the length and 4 elements along the arc. Results are shown in Figure 10 for both the adaptive procedure and the uniform fine mesh. Good agreement is observed for the first case, while the adaptive procedure is slightly less accurate for the second case. It is observed that the steady-state moment value changes considerably between the two cases. The speedup factor of the adaptive procedure compared to using a uniform mesh with similar accuracy is given in Table 2. Similar speedups are obtained for both cases, although in the second case this speedup is achieved with less accuracy.

D. Influence of element length limit

We now consider tape springs with the properties given in Table 1 and two sets of radii and thicknesses, given in Table 3. Using Eq. (8), the element length limit is $h_{th} = 1.2$ mm for the first case and $h_{th} = 1.4$ mm for the second case. The initial mesh is the same as before, with 4 elements along the length and 4 elements along the arc. Results are shown in Figure 11 for both the adaptive procedure and the uniform fine mesh. The speedup factor of the adaptive
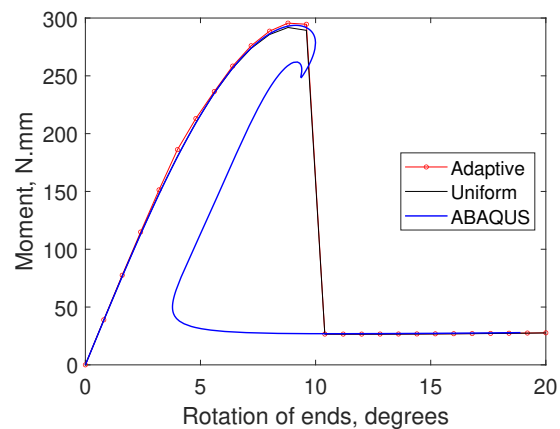

Fig. 6   **Moment-rotation plots for tape spring with parameters $L = 300$ mm, $R = 10$ mm and $t = 0.1$ mm.**
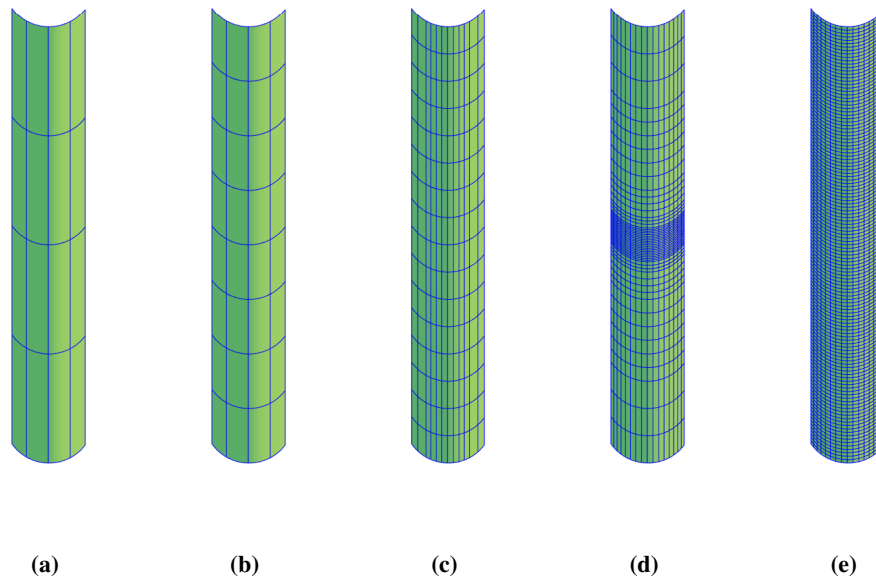
6

Fig. 7 Meshes at different rotation angles from adaptive meshing simulation shown in Figure 6 and uniform mesh. (a) Initial mesh (16 elements). (b) 2.4° rotation (32 elements). (c) 5.6° rotation (192 elements). (d) 10.4° rotation (832 elements). (e) Uniform mesh (2048 elements).

.

Table 1 Speedup factors for three tape springs with different lengths.

Properties	Speedup Factor
$R = 10$ mm, $t = 0.1$ mm, $L = 150$ mm	3.4
$R = 10$ mm, $t = 0.1$ mm, $L = 300$ mm	4.7
$R = 10$ mm, $t = 0.1$ mm, $L = 600$ mm	10.6

procedure compared to using a uniform mesh with similar accuracy is given in Table 3. It is observed that less accuracy is obtained than in previous cases, although the speedup factor is higher. This hints at the use of a smaller refinement indicator threshold r_0 in order to get more accurate results while keeping good computational speed.

VI. Conclusion

A new adaptive meshing procedure for deployable thin shell structures has been presented. By using one refinement indicator per element axis, the refinement procedure can be oriented along a particular axis. This is useful since refining in every direction is not always the optimal choice. In addition, this type of refinement is convenient for use with isogeometric finite elements that use NURBS shape functions. A refinement limit specific for tape springs has also been introduced based on an estimate of the boundary layer effect of the fold. Test cases have analyzed the effects of various

Table 2 Speedup factors for two tape spring geometries with the same element length limit.

Properties	Speedup Factor
$R = 6$ mm, $t = 0.15$ mm, $L = 300$ mm	2.2
$R = 15$ mm, $t = 0.06$ mm, $L = 300$ mm	2

7

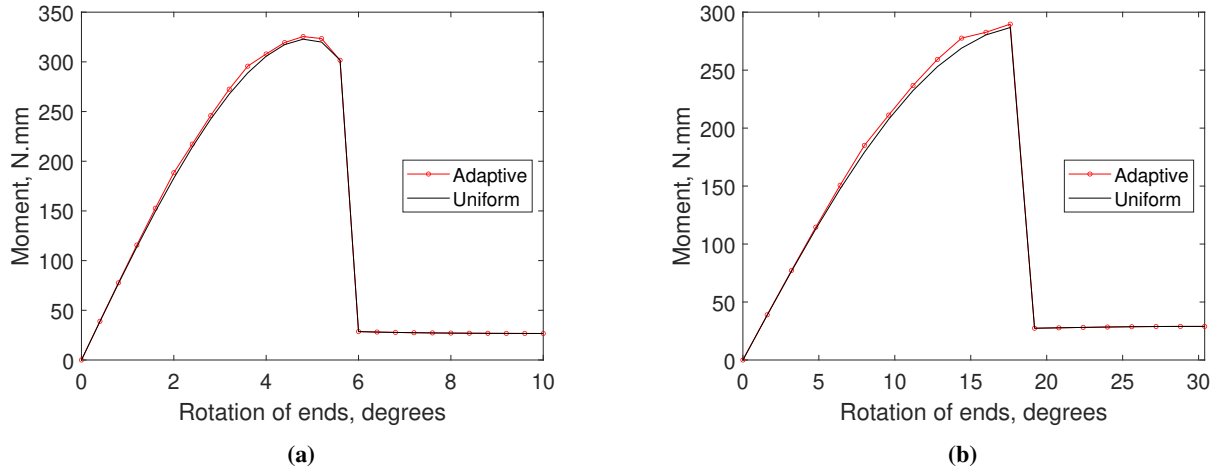**(a)**   **(b)**

Fig. 8   **Moment-rotation plots for tape springs with parameters $R = 10$ mm, $t = 0.1$ mm and different lengths. (a)** $L = 150$ **mm. (b)** $L = 600$ **mm.**

.

Table 3   **Speedup factors for two tape spring geometries with different element length limit.**

Properties	Speedup Factor
$R = 15$ mm, $t = 0.1$ mm, $L = 300$ mm	4.2
$R = 20$ mm, $t = 0.1$ mm, $L = 300$ mm	3.6

geometrical parameters.

The proposed adaptive procedure performs well for the tape springs considered. It is particularly efficient when the tape spring is long relative to its cross-section dimensions. The radius and thickness seem to have little influence on the accuracy of the adaptive method if the element length limit, as defined by Equation 8, is kept fixed. However, if the element length limit is increased from the baseline case presented, less accurate results have been observed (although with even higher speedup factors). This might indicate that the optimal value of the refinement indicator threshold r_0 used to mark refinement depends on the element length limit h_{th}.

Further work should consider dynamic analysis of tape springs as well as more complex structures. The use of T-splines should also be considered.

Acknowledgments

References

[1] Glaser, P. E., "Power from the sun: Its future," *Science*, Vol. 162, No. 3856, 1968, pp. 857–861.

[2] Kiper, G., and Soylemez, E., "Deployable space structures," *2009 4th International Conference on Recent Advances in Space Technologies*, IEEE, 2009, pp. 131–138.

[3] Calladine, C., and Seffen, K., "Folding the Carpenter's tape: boundary layer effects," *Journal of Applied Mechanics*, Vol. 87, No. 1, 2020.

[4] Bathe, K.-J., *Finite element procedures*, Prentice Hall, 2006.

[5] Lo, S., "Finite element mesh generation and adaptive meshing," *Progress in Structural Engineering and Materials*, Vol. 4, No. 4, 2002, pp. 381–399.
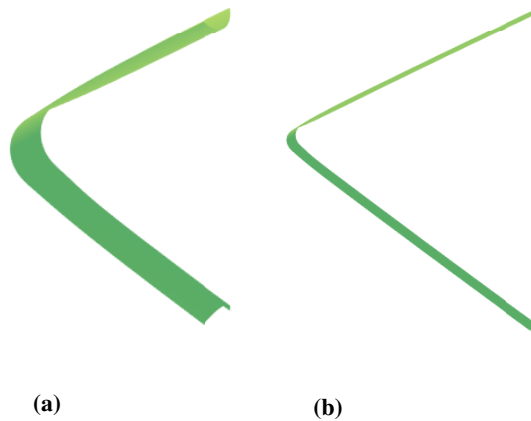
Fig. 9 Tape spring with ends rotated 60 ° and parameters $R = 10\,\text{mm}$ **and** $t = 0.1\,\text{mm}$. **(a)** $L = 150\,\text{mm}$. **(b)** $L = 600\,\text{mm}$.

[6] Ainsworth, M., and Oden, J. T., "A posteriori error estimation in finite element analysis," *Computer Methods in Applied Mechanics and Engineering*, Vol. 142, No. 1-2, 1997, pp. 1–88.

[7] Mosler, J., and Ortiz, M., "Variational h-adaption in finite deformation elasticity and plasticity," *International Journal for Numerical Methods in Engineering*, Vol. 72, No. 5, 2007, pp. 505–523.

[8] Luo, Y., "Adaptive nearest-nodes finite element method guided by gradient of linear strain energy density," *Finite elements in analysis and design*, Vol. 45, No. 12, 2009, pp. 925–933.

[9] Sze, K., and Zhou, Y., "An efficient rotation-free triangle for drape/cloth simulations—part I: model improvement, dynamic simulation and adaptive remeshing," *International Journal of Computational Methods*, Vol. 13, No. 03, 2016, p. 1650021.

[10] Hughes, T. J., Cottrell, J. A., and Bazilevs, Y., "Isogeometric analysis: CAD, finite elements, NURBS, exact geometry and mesh refinement," *Computer Methods in Applied Mechanics and Engineering*, Vol. 194, No. 39-41, 2005, pp. 4135–4195.

[11] Uhm, T.-K., and Youn, S.-K., "T-spline finite element method for the analysis of shell structures," *International Journal for Numerical Methods in Engineering*, Vol. 80, No. 4, 2009, pp. 507–536.

[12] Dörfel, M. R., Jüttler, B., and Simeon, B., "Adaptive isogeometric analysis by local h-refinement with T-splines," *Computer methods in applied mechanics and engineering*, Vol. 199, No. 5-8, 2010, pp. 264–275.

[13] Wang, P., Xu, J., Deng, J., and Chen, F., "Adaptive isogeometric analysis using rational PHT-splines," *Computer-Aided Design*, Vol. 43, No. 11, 2011, pp. 1438–1448.

[14] Kiendl, J., "Isogeometric analysis and shape optimal design of shell structures," Ph.D. thesis, Technische Universität München, 2011.

[15] Seffen, K., and Pellegrino, S., "Deployment dynamics of tape springs," *Proceedings of the Royal Society of London. Series A: Mathematical, Physical and Engineering Sciences*, Vol. 455, No. 1983, 1999, pp. 1003–1048.

[16] Nocedal, J., and Wright, S., *Numerical optimization*, Springer Science & Business Media, 2006.

[17] De Borst, R., Crisfield, M. A., Remmers, J. J., and Verhoosel, C. V., *Nonlinear finite element analysis of solids and structures*, John Wiley & Sons, 2012.
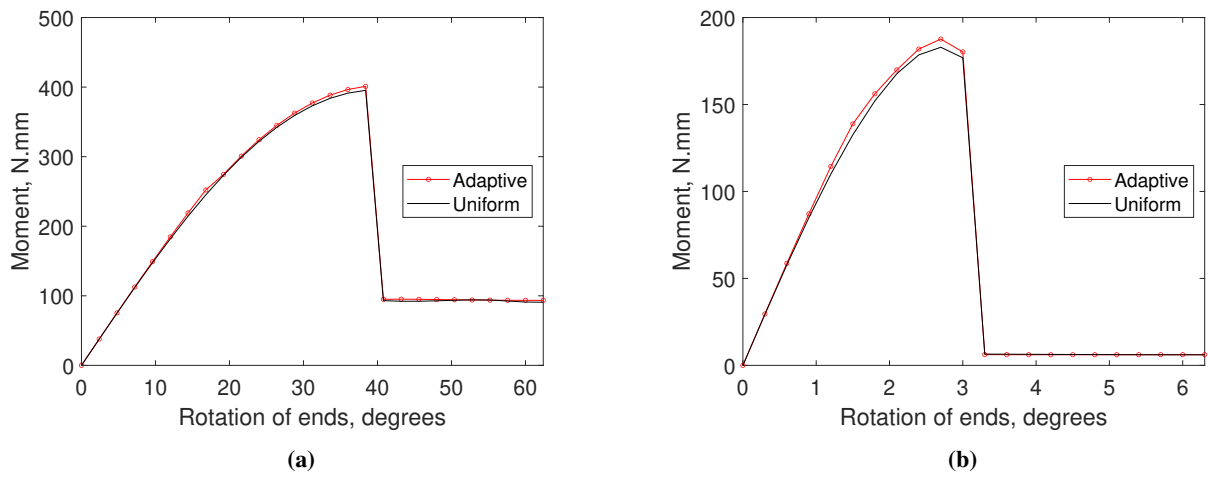
(a)   **(b)**

Fig. 10   **Moment-rotation plots for tape springs with** $L = 300$ **mm and different radii and thicknesses.** **(a)** $R = 6$ **mm**, $t = 0.15$ **mm.** **(b)** $R = 15$ **mm**, $t = 0.06$ **mm.**

.

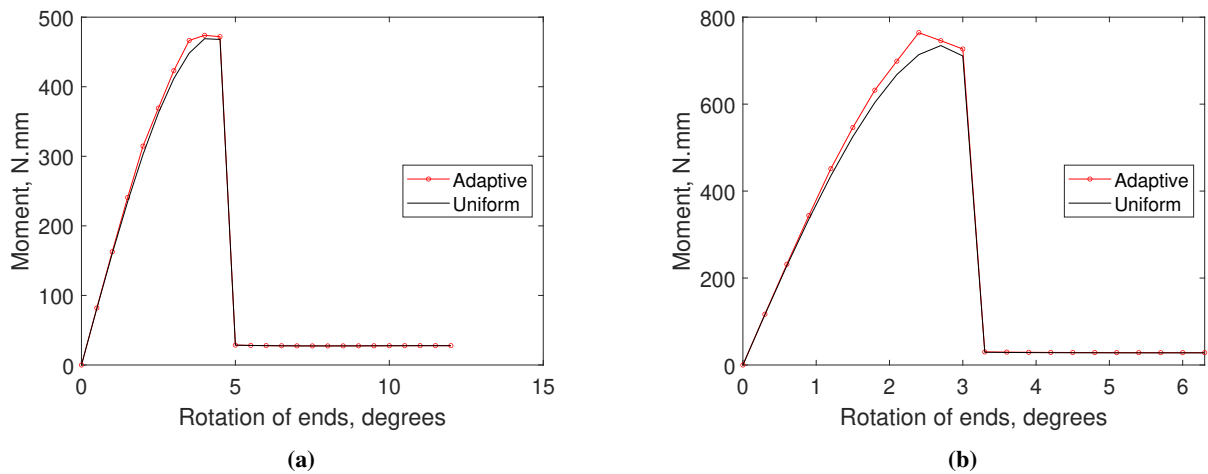

(a)   **(b)**

Fig. 11   **Moment-rotation plots for tape springs with** $L = 300$ **mm and variable element length limit.** **(a)** $R = 15$ **mm**, $t = 0.1$ **mm.** **(b)** $R = 20$ **mm**, $t = 0.1$ **mm.**

.

10